Uncertainty Analysis of Laminar Aeroheating Predictions for Mars Entries

Deepak Bose,[†] and Michael Wright[*]
NASA Ames Research Center, Moffett Field, CA 94035

Abstract

A Monte Carlo sensitivity and uncertainty analysis is performed for a laminar convective heating prediction in a moderate Mars atmospheric entry condition using a state-of-the-art computational fluid dynamics (CFD) code. The objectives are to isolate the rate limiting mechanisms and identify the chief sources of aeroheating uncertainty. A flux based wall catalysis formulation is used to define four different catalytic regimes that are then individually analyzed. A total of 130 CFD input parameters are statistically varied to shortlist a handful of parameters that essentially control the heat flux prediction. The uncertainties in these key input parameters are estimated, and a full Monte Carlo uncertainty analysis is performed. The results obtained provide the quantitative contribution of uncertainties in key modeling parameters, such as collision integrals, wall catalysis, reaction rates, etc. to the final heat flux uncertainty. It is found that in high and low catalytic regimes, the collision integrals (which govern the transport properties of the mixture) contribute a large portion of the uncertainty, while in the moderately catalytic regime the catalytic properties of the surface contribute almost all of the uncertainty.

Introduction

NASA's Mars Technology Program is actively pursuing development and selection of technologies for several proposed Mars exploration missions scheduled to launch during the next several years. NASA's new Vision for Space Exploration also calls for robotic exploration of Mars to lay the groundwork for possible human expeditions. In addition NASA's In-Space Propulsion Program is considering aerocapture missions to Mars, among many destinations, as a means to reduce the on-board propellant requirement (and resulting system mass) for orbital insertion of an arriving vehicle.[1] An aerocapture vehicle is subjected to aerothermal heating as it dissipates the vehicle kinetic energy at the destination planet using atmospheric drag. The performance of this technology is determined by the propellant mass savings as compared to the mass of the vehicle thermal protection system (TPS). For both aerocapture and direct entry the selection of an appropriate TPS material, as well as the required thickness (mass) of the TPS for each mission, are determined by the aerothermal environment encountered by the vehicle during the entry. Clearly, aeroheating predictions and their associated uncertainties for Mars entries will be necessary for design and development of thermal protection systems for a variety of missions.

A large number of investigators have performed aerothermal analysis of Mars entry environments using state-of-the-art CFD codes.[2-4] Although CFD simulations provide aeroheating predictions with a greater level of fidelity than simple engineering correlations, the confidence level associated with these predictions remains largely unknown, especially in the regimes where validation with ground test or flight data has not been possible. It is well known that aeroheating predictions made from these CFD analyses are sensitive to the physical, chemical, and numerical models employed. The uncertainty in these predictions, which is a critical element of the overall entry system risk, is the result of a combined effect of parametric and structural uncertainties in the underlying models. Parametric uncertainties are due to imprecise measurements or estimates of input parameters, such as reaction rates, thermal relaxation times, transport

[†] Senior Research Scientist, ELORET Corporation, dbose@arc.nasa.gov. Member AIAA
[*] Senior Research Scientist, Reacting Flow Environments Branch, MS 230-2. Senior Member AIAA

properties, and wall catalycity. Structural uncertainties, on the other hand, are caused by deficiencies in the formulation of the physical and numerical models intended to represent the true environment. Although prior aerothermal investigations recognize these uncertainties, there have been few rigorous attempts to quantify them and assess their effect on the final aeroheating uncertainty. For the purposes of design and system risk assessment, the uncertainty limits associated with an aeroheating prediction are almost as important as the aeroheating value itself, especially when the limits are large. Without a formal uncertainty analysis, the sub-system risk estimate remains crude, which may result in misplaced priorities in the overall system risk reduction strategy.

In this work, we carry out a systematic Monte Carlo uncertainty and sensitivity analysis for Mars entry aerothermodynamics at moderate entry conditions. A similar uncertainty analysis was performed for Titan entry vehicle to ascertain the uncertainty associated with radiative heating at the stagnation point.[5] This work will focus on non-ablating, laminar convective heating rates in the forebody of a rigid aeroshell. Apart from quantifying the uncertainty in the aeroheating predictions, this technique will allow us to isolate the chief sources of uncertainty in the models. These uncertainty drivers can then be prioritized and targeted for further ground based investigation or proposed flight instrumentation to maximize return from research. A sensitivity analysis, which is a by-product of the uncertainty analysis, will also provide valuable insights by identifying the rate-limiting steps and dominant mechanisms. The results of this sensitivity analysis can also be used to identify potential structural uncertainties in the current aeroheating models; if the models employed are correct the sensitivities predicted should be reproducible via targeted experiments.

Among the physical phenomena that play a critical role in the laminar heating rates in the absence of shock layer radiation and TPS ablation are wall catalysis, boundary layer transport, and chemical kinetics. Each of these phenomena will be explored in this work. The rest of this paper describes the baseline model and the entry conditions used, followed by a sensitivity analysis to identify a key set of input parameters. This is followed by an estimate of uncertainties that exist in these key parameters. Finally, we perform a Monte Carlo uncertainty analysis to track the impact of these uncertainties on forebody heat flux.

Baseline Conditions and Model

A. Mars Pathfinder Entry Conditions

The primary focus of the analysis in this work will be the Mars Pathfinder entry vehicle, which entered the atmosphere of Mars on July 4, 1997 at a relative velocity of 7.5 km/s.[6] Mars Pathfinder is a good test case because it was a ballistic (non-lifting) entry at a velocity for which convective heating was large but radiative heating was small. The test case allows us to explore moderate entry conditions where convective heating dominates, without the added complexities of shock layer radiation, which becomes critical only at higher speeds. The analysis in this work will be performed at the peak heating condition on the entry trajectory:[4]

$$\rho_0 = 2.8\times10^{-4}\ kg/m^3, \quad u = 6.596\ km/s, \quad T = 169\ K$$

for which pre-flight calculations,[4] assuming a fully catalytic surface, predicted a peak convective heat flux of approximately 110 W/cm^2. The forebody of the Pathfinder entry vehicle was a 70.2 degree axisymmetric sphere-cone with a rounded shoulder as shown in Fig. 1. A post-flight analysis of temperature sensor data concluded that at the stagnation point the temperature data are consistent with a peak heat flux during entry of about 85% of the predicted fully catalytic laminar heating.[4]

B. Numerical and Physical Models

The flowfield computations in this work are performed using the computational fluid dynamics (CFD) code DPLR.[7] DPLR is a parallel multiblock finite-volume code that solves the Navier-Stokes equations including finite-rate chemistry and the effects of thermal nonequilibrium. DPLR, along with the code LAURA,[8] are the primary tools currently used within NASA for aerothermal analysis of Earth and planetary entry

vehicles. In addition to the conservation equations for mass and momentum, two energy equations are solved; a total energy equation and a combined vibro-electronic energy equation. In this formulation it is assumed that the vibrational and electronic modes of the gas are in equilibrium with each other, but not with the translational-rotational component. The energy exchange between the translational-rotational and vibrational-electronic modes is modeled using a Landau-Teller formulation assuming simple harmonic oscillators. Vibrational relaxation times are obtained from Millikan and White[9] for most species. Data from Camac[10] are used for vibrational relaxation times of CO_2 and CO. A single vibrational temperature is used for all polyatomic species. Characteristic vibrational temperatures for the simple harmonic oscillator approximation are taken from Gurvich et al.[11]

Viscosity and thermal conductivity are modeled using the species expressions and mixing rules presented by Gupta et al.[12] Required collision integrals are taken from Wright and Bose[13] and Wright et al.[14] for all binary interactions. The self-consistent effective binary diffusion (SCEBD) method[15] is used to model mass diffusion fluxes.

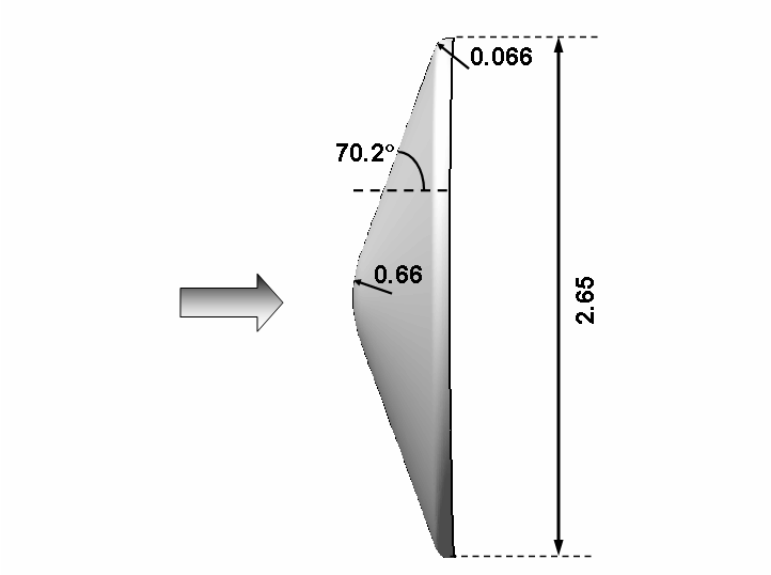

Figure 1. 70.2° sphere cone Mars Pathfinder aeroshell.

B. Chemical Kinetics Model

The Martian atmosphere consists of approximately 97% CO_2 and 3% N_2 by volume, with trace amounts of other species (primarily Ar). A review of the nonequilibrium kinetics of a shock heated mixture of CO_2–N_2 was first presented by Park *et al.*[16] for 18 species (CO_2, NCO, CO, CO^+, CN, NO, NO^+, N_2, O_2, O_2^+, C_2, N, N^+, C, C^+, O, O^+, e) with ionization. Mitcheltree and Gnoffo[3] subsequently presented a reduced 8 species (CO_2, CO, NO, N_2, O_2, N, C, O) mechanism that neglected ionization. The reactions included in these mechanisms are listed in Table I. The rates of the common reactions are taken from Park *et al.*[16] At the conditions of interest in the present paper the level of ionization in the flowfield is extremely small. Therefore, it is expected that the heat flux computed using the Mitcheltree and Gnoffo 8-species model should be an accurate representation of the flowfield. In order to test the validity of this assumption, a calculation was performed using each model at the trajectory point discussed above for fully catalytic and non-catalytic conditions. Figure 2 demonstrates that the convective heating rates predicted by the 8 and 18-species models are nearly identical, with a maximum difference of 3% at the stagnation point for the fully catalytic condition. Based on this result the 8-species model is used for all cases presented in this paper.

It should be noted that the rates of many of these reactions have not been directly measured at conditions relevant to Martian entry. Some are estimated from indirect observations, while other are pure estimates,[16] which make them sources of uncertainty. The uncertainties in the relevant reactions will be discussed in a later section.

Table I. The reaction mechanisms for Mars entry shock layer, obtained from Refs. 16 and 3.

	Chemical Reactions	Park 18 sp.	Mitcheltree and Gnoffo 8 sp.
1	$CO_2 + M \Leftrightarrow CO + O + M$	×	×
2	$CO + M \Leftrightarrow C + O + M$	×	×
3	$N_2 + M \Leftrightarrow 2N + M$	×	×
4	$O_2 + M \Leftrightarrow 2O + M$	×	×
5	$NO + M \Leftrightarrow N + O + M$	×	×
6	$C_2 + M \Leftrightarrow 2C + M$	×	
7	$CN + M \Leftrightarrow C + N + M$	×	
8	$NCO + M \Leftrightarrow CO + N + M$	×	
9	$C + e \Leftrightarrow C^+ + 2e$	×	
10	$O + e \Leftrightarrow O^+ + 2e$	×	
11	$NO + O \Leftrightarrow O_2 + N$	×	×
12	$N_2 + O \Leftrightarrow NO + N$	×	×
13	$CO + O \Leftrightarrow O_2 + C$	×	×
14	$CO + C \Leftrightarrow C_2 + O$	×	
15	$CO + N \Leftrightarrow CN + O$	×	
16	$CO + N \Leftrightarrow NO + C$		×
16	$N_2 + C \Leftrightarrow CN + N$	×	
17	$CN + O \Leftrightarrow NO + C$	×	
18	$CN + C \Leftrightarrow C_2 + N$	×	
19	$CO_2 + O \Leftrightarrow O_2 + CO$	×	×
20	$CN + O_2 \Leftrightarrow NCO + O$	×	
21	$CN + CO_2 \Leftrightarrow NCO + CO$	×	
22	$CN + NO \Leftrightarrow NCO + N$	×	
23	$CO + NO \Leftrightarrow NCO + O$	×	
24	$CO + NO \Leftrightarrow CO_2 + N$		×
24	$CO + CO \Leftrightarrow CO_2 + C$		×
24	$CN + CO \Leftrightarrow NCO + C$	×	
25	$N + O \Leftrightarrow NO^+ + e$	×	
26	$O + O \Leftrightarrow O2^+ + e$	×	
27	$C + O \Leftrightarrow CO^+ + e$	×	
28	$NO^+ + C \Leftrightarrow NO + C^+$	×	
29	$O_2^+ + O \Leftrightarrow O^+ + O_2$	×	
30	$NO^+ + N \Leftrightarrow O^+ + N_2$	×	
31	$NO^+ + O \Leftrightarrow O_2^+ + N$	×	
32	$CO + C^+ \Leftrightarrow CO^+ + C$	×	
33	$O_2 + C^+ \Leftrightarrow O_2^+ + C$	×	

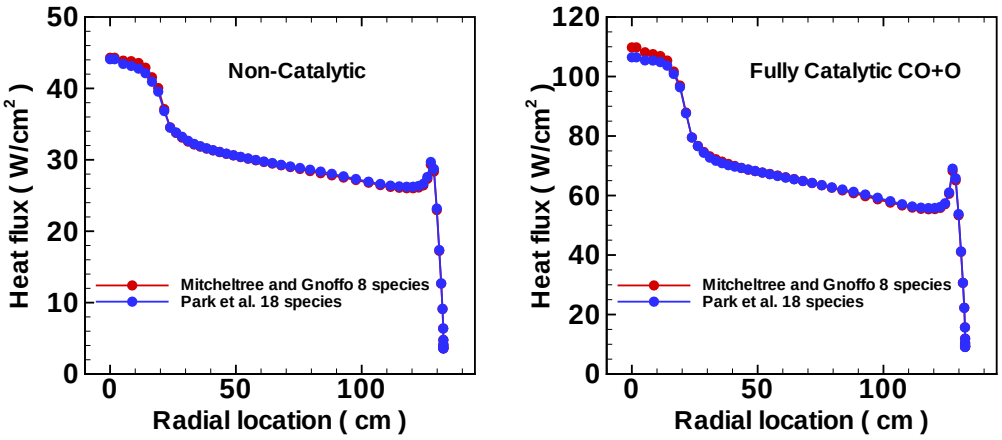

Figure 2. Laminar convective heat flux on the forebody at the baseline conditions. The effect of different chemical kinetics model in the heat flux is shown. (a) Non-catalytic wall assumed and (b) fully catalytic wall assumed.

C. Catalysis Model

It is well known that the recombination of atoms and radicals due to the catalytic activity of the wall is often a primary source of convective heating. However, the mechanism involved in the catalytic recombination is poorly understood, in part due to difficulties in performing surface diagnostics at appropriate temperature and pressure. In addition, the surface condition due to past history and exposure to other adsorbing species also alters the catalytic properties, making it further difficult to quantify and address flight traceability issues. Consequently, modeling of catalytic reactions at the surface has been relatively primitive. In fact, for Mars entries the so-called supercatalytic wall model is frequently employed,[17] in which the gas composition at the surface is specified to be equal to that in the freestream. This model, while it provides a conservative estimate of the heating rate, only accounts for limiting of the recombination processes by diffusion transport of participating species through the boundary layer to the surface. The catalytic models are incorporated in the CFD via boundary conditions that are applied to the species mass and the total energy equations. In this work a radiative wall equilibrium energy boundary condition is used for the total energy equation.

In general, surface catalytic reaction models solve a surface site balance equation coupled with gas phase densities. However, these models assume a heterogeneous reaction model, such as the Langmuir-Hinshelwood (LH) or Eley-Rideal (ER) mechanisms. In the LH model the participating recombining species are first adsorbed on the surface before recombining and desorbing into the gas phase, while in the ER mechanism a gas phase species recombines directly with an adsorbed species. Several simulations of Mars entry aerothermodynamics have assumed an ER mechanism to describe wall catalysis because of its simplicity. For example, in the Mitcheltree and Gnoffo wall catalysis model CO + O recombination is assumed to occur on the surface via a two-step ER process.[3]

However, the literature indicates that the LH mechanism is more commonly observed than the ER mechanism.[18] In fact, direct experimental evidence of ER mechanism under any condition is lacking. For the well studied catalytic reaction of CO oxidation on transition metal surfaces, especially the platinum group metals, the LH mechanism is observed to occur. The LH mechanism is also found to govern other catalytic reactions such as CO hydrogenation on metallic surfaces.[18] Therefore, the use of the ER mechanism to describe surface catalysis adds uncertainty that is difficult to assess, especially since experiments measuring catalytic properties of carbon based materials in a dissociated Mars environment have never been performed under re-entry conditions.

For this work we use a simplified flux based surface species recombination model that does not rely on a specific heterogeneous reaction model such as the LH or ER mechanism. We know that for Mars entry, at the conditions of interest, the freestream CO_2 is almost completely dissociated into CO and O, while most

of the CO formed remains undissociated. Therefore the composition at the boundary layer edge consists primarily of CO+O with the possibility of additional species appearing via recombination. Among the several recombination reactions possible at the wall, the following two involving the dominant species have been proposed[3-4,19] as the reactions that are likely to control the catalytic heating of the vehicle

$$\mathrm{CO} + \mathrm{O} \xrightarrow{\gamma_1} \mathrm{CO_2} \quad , \Delta E = 5.51\,\mathrm{eV} \tag{1}$$

$$\mathrm{O} + \mathrm{O} \xrightarrow{\gamma_2} \mathrm{O_2} \quad , \Delta E = 5.16\,\mathrm{eV} \tag{2}$$

Other recombination reactions are also possible but due to their low reactant densities in the boundary layer, the resulting effect on catalytic heating will be small. The parameters γ_1 and γ_2 are the reaction probabilities for reactions (1) and (2) respectively. However, these parameters do not vary independently, since both reactions consume O atoms. From kinetic theory the incoming flux at the wall for a given species *s* with number density n_s is written as

$$\Gamma_s^+ = n_s u_s \,, \tag{3}$$

where u_s is the quarter of the thermal speed of the species [$u_s = (R_s T/2\pi M_s)^{1/2}$]. If γ_O is assumed to be the fraction of O atoms that are lost via either reaction (1) or (2) after they strike the surface, the net O atom flux at the wall is written as

$$\Gamma_O = \gamma_O n_O u_O \tag{4}$$

Let us first consider the case when reaction (1) is CO flux limited, i.e. $n_{CO} u_{CO} < n_O u_O$. For this case, the O atom flux at the wall is the sum of the contributions of reactions (1) and (2),

$$\Gamma_O = \gamma_1 n_{CO} u_{CO} + \gamma_2 n_O u_O \tag{5}$$

From (4) and (5) we can write γ_O as

$$\gamma_O = \gamma_1 \frac{n_{CO} u_{CO}}{n_O u_O} + \gamma_2 \tag{6}$$

We now define a preference factor for O+O recombination as p_2 (= γ_2/γ_O), which represents the ratio of the flux of O atoms consumed by the O+O recombination to the total flux of O atoms consumed by either process. For a given value of p_2 the maximum consumption of O atoms is limited by CO density, and is given by

$$\gamma_{O,\max} = \min\left[\frac{1}{1-p_2}\left(\frac{n_{CO} u_{CO}}{n_O u_O} \right) \;,\; 1 \right] \tag{7}$$

We further define a catalytic parameter γ_{cat} as the ratio of actual to the maximum possible O atom consumption. Therefore,

$$\gamma_{cat} = \frac{\gamma_O}{\gamma_{O,\max}} \tag{8}$$

Next we consider the case when reaction (1) is O flux limited, i.e. $n_O u_O < n_{CO} u_{CO}$. We note that in this case $\gamma_{O,max}$ is always 1. The sum of the contributions of both reactions to O atom flux is written as

$$\begin{aligned} \Gamma_O &= \gamma_1 n_O u_O + \gamma_2 n_O u_O \\ \gamma_O &= \gamma_1 + \gamma_2 \end{aligned} \tag{9}$$

In each case the value of γ_{cat} can vary between 0 (corresponding to a non-catalytic wall from which all O atoms are reflected), to 1 (corresponding to a fully catalytic wall at which maximum possible O atoms recombine via reaction (1) and (2)). It is also evident that since there are two competing reactions consuming O atoms, the catalytic heating will depend on the relative preference of one channel over the other due to their different stoichiometric requirements. The difference in the heats of formation is only about 6%. We also note that the preference factor, p_2, which determines the fraction of recombining O atoms that result in O_2 formation [reaction (2)], also varies between 0 and 1. By varying the parameters γ_{cat} and p_2 independently between 0 and 1, the entire window of catalycity can therefore be spanned. For example, setting $\gamma_{cat} = 0$ results in a non-catalytic surface regardless of the value of p_2. The fully catalytic limit of the Mitcheltree model can be reproduced by setting $\gamma_{cat} = 1$ and $p_2 = 0$. Therefore, thoughout this paper we will use γ_{cat} and p_2 as the preferred set of input variables instead of γ_1 and γ_2 that cannot be varied independently between well defined limits. The transformations, regardless of which species is limiting, can be written as

$$\gamma_1 = \gamma_{cat}\,\gamma_{O,max}(1-p_2)\max\left[\frac{n_O u_O}{n_{CO} u_{CO}}\quad,\quad 1\right] \qquad (10)$$

$$\gamma_2 = \gamma_{cat}\,\gamma_{O,max}\,p_2$$

The form of fluxes can also be written, in terms of these two parameters, as

$$\begin{aligned}\Gamma_O &= \gamma_{cat}\gamma_{O,max} n_O u_O \\ \Gamma_{CO} &= (1-p_2)\Gamma_O \\ \Gamma_{CO_2} &= \Gamma_{CO} \\ \Gamma_{O_2} &= \frac{1}{2} p_2 \Gamma_O\end{aligned} \qquad (11)$$

The above equation set can be used to model wall catalycity without being limited by the assumption of a particular site balance reaction model. The drawback of this approach is that γ_{cat} and p_2 remain as unknown parameters with unknown dependencies on factors like temperature, densities, surface condition, etc. Such dependencies can somewhat be described by a chosen surface site balance model, however, the validity of such models, especially the commonly used ER model is unknown. Therefore, in this work we will deal with γ_{cat} and p_2 that have clear physical interpretations and can be varied independently between well defined limits.

D. Heat flux variation due to wall catalytic parameters

We now present the variation of stagnation point heat flux with the catalytic parameters γ_{cat} and p_2 defined in the last section. Figure 3(a) shows the variation of the stagnation point heat flux, q_w, with catalytic efficiency, γ_{cat} at two extremes of p_2. The curves in Fig. 3(a) show three distinct regimes of heat flux sensitivity to catalycity. The first is the high catalytic efficiency region (γ_{cat}>0.1), where the heat flux weakly varies with the value of γ_{cat} because the recombination rate is limited by the transport (diffusion) of reactants (CO and O) through the boundary layer to the wall. An important consequence of the diffusion limiting phenomenon is that for heat shield design, it is not critical to know that exact value of catalytic efficiency, γ_{cat}, as long as it is confirmed that the catalytic efficiency is high. However, it should be emphasized that even in the diffusion limited regime a precise determination of the preference factor p_2 may still be necessary, as seen by the large difference between the p_2=0 and p_2=1 heat flux levels in Fig. 3(a). This will be further discussed later in this section. The second region in Fig. 3(a) is the moderate catalytic efficiency regime ($10^{-3} < \gamma_{cat} < 10^{-1}$). In this regime, the heat flux is highly sensitive to the exact value of γ_{cat} as the recombination rate is surface process rate limited. In this regime a precise determinations of γ_{cat} and p_2 are essential for heat flux computation. The third region in Fig. 3(a) is the weakly catalytic regime ($\gamma_{cat} < 10^{-3}$), where, again, the exact value of γ_{cat} is unimportant to heating since wall catalycity contributes little to the heating as compared to the thermal conduction from the hot gas. These three

catalytic regimes will be frequently referred to throughout this paper as the sensitivity and uncertainty analyses are performed separately for each of these regimes.

Figure 3(b) shows the variation of the stagnation point heat flux, q_w, versus the preference factor, p_2, assuming a fully catalytic wall (γ_{cat} =1). The parameter p_2 represents the importance of O+O→O_2 channel as compared to CO+O→CO_2 reaction channel. It is useful to emphasize that although CO oxidation by adsorbed O atoms has been well studied on transition state metals for catalytic converter applications, CO+O recombination was found not to occur at detectable levels on quartz surfaces analyzed by Sepka et al.[20] and Kolesnikov.[21] The O+O recombination however, was detected in the presence of CO on these surfaces in both investigations. This raises the question whether CO+O recombination is likely to occur in flight where the surface temperature is well above 1000 K. In this work we treat this as an uncertainty by varying p_2. In addition to q_w, Fig. 3(b) also shows the gas phase number densities of CO and O at the stagnation point. When p_2 is low, CO+O recombination is dominant, and both CO and O are efficiently utilized. This efficient utilization of both species occurs because the shock layer number densities of these species are similar in magnitude, (since they are produced by direct dissociation of CO_2) which is appropriate for the 1:1 stoichiometric ratio required for CO+O recombination. Figure 3(b) shows that a slight excess of O atoms (caused due to a faster diffusion of lighter O atoms compared to CO) is seen. The extra O atoms can be further utilized if a small amount of O+O recombination is allowed to occur by raising p_2. This trend is evident in Fig. 3 (b) as a drop in O density and a further rise of q_w as p_2 is raised from a low value to 10^{-1}. This value of q_w is the most conservative estimate possible using the current catalytic mechanism and represents the maximum utilization of CO and O. Once p_2 is raised above this critical value, the catalytic heating begins to sharply fall. This drop occurs because the stoichiometric requirement of the catalytic reactions no longer matches the available number density ratio of CO and O. As a result a rise in p_2 is accompanied by an under utilization of CO manifested as a rise in its density. At the extreme of p_2=1, when only O atoms are utilized and CO molecules are reflected back, consequently the catalytic heating level is at its minimum while still assuming γ_{cat} =1.

In order to obtain a conservative estimate in design, often a supercatalytic wall assumption is employed.[17] This assumption requires that upon diffusion to the wall, the species mass fractions recover the freestream composition, which maximizes the recovery of chemical enthalpy on the surface. For the Mars Pathfinder simulations in this work, the supercatalytic heat flux is about 120 W/cm^2. This value, which is about 5 W/cm^2 higher than the maximum obtained via the catalytic mechanism defined in Section C, is shown in Fig. 3(a) as a horizontal line. Although this assumption is a useful design tool since it gives a ceiling for catalytic heating, it may also be unphysical. Since the species mass fractions are imposed at the wall, the net flux of a species may be higher than what is allowed by kinetic theory [see Eq. (3)]. The only limiting phenomenon in a supercatalytic assumption is the diffusion process. Nevertheless, we will consider this limiting case along with high, moderate, and low catalytic regimes

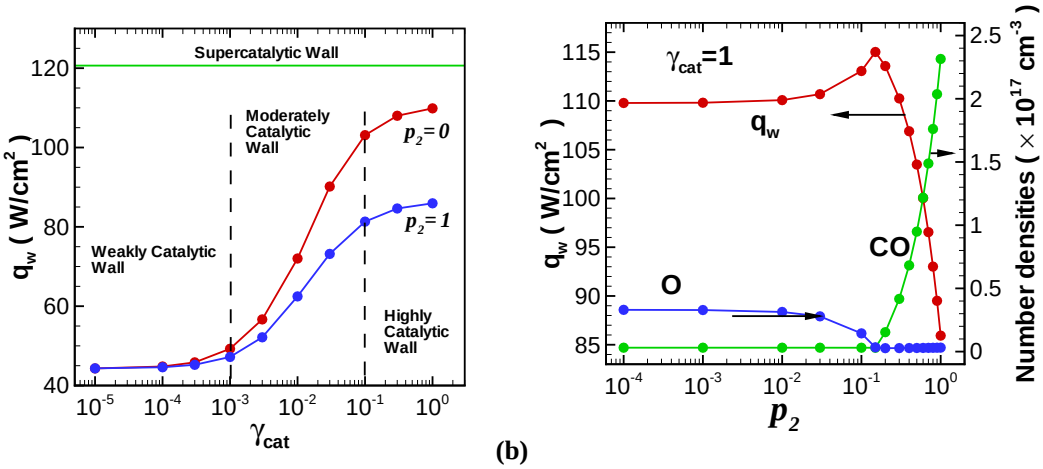

(a) (b)

Figure 3 (a) Stagnation point heat flux variation with different levels of wall catalycity and preference factors and (b) variations of heat flux and wall number densities of gas phase CO and O with the preference parameter p_2, (γ_{cat} =1).

Methodology

A Monte Carlo sensitivity and uncertainty analysis involves statistically varying the input parameters and tracking changes in the output of interest, in this case, the heat flux q_w. The details of the methodology can be found in Ref. 5. For the sake of completeness we briefly outline the steps involved in this work.

1. Input variables that need to be varied are first identified. In DPLR, or any aerothermal CFD code for that matter, the input variables can be categorized as reaction rate parameters, vibration-dissociation coupling parameters, vibrational-translational relaxation times, binary interaction collision integrals for transport property calculations (diffusion, viscosity, and thermal conductivity coefficients), and wall catalycity parameters. Since this work focuses only on laminar, non-blowing convective heating predictions, input parameters that relate to bulk material properties, material response and turbulence models are not considered. For an 8-species kinetic model, 130 input parameters, as shown in Table II, are independently varied in this work.
2. Variability limits for these input parameters are chosen that roughly represent their typical uncertainties. The chosen variability limits do not represent the true estimated input uncertainties since they will be used for sensitivity analysis. We vary each input parameter independently and symmetrically about their baseline values using a Gaussian distribution. The only exceptions are the catalytic parameters γ_{cat} and p_2. These parameters are varied within the variability limits (to be specified based on the catalytic regime) using a uniform distribution on a log scale. The models used and the parameters varied are also shown in Table II.
3. Independent input sets generated by varying the parameters are used to make DPLR runs to obtain corresponding heat flux values. In this work a total of 3000 axisymmetric runs are made for each catalytic regime in order to get statistical accuracy.
4. Input-output correlation coefficients are computed using linear regression analysis and the fractional contribution of each input variability to the overall output variability is obtained. The largest contributors are the ones that cause the most sensitivity to heat flux. This allows us to shortlist a handful of the parameters out 130 considered.
5. For the shortlisted input parameters, an estimate of their associated uncertainties is done.
6. All input parameters are again varied over the previously chosen limits, except the shortlisted input parameters, for them the limits are adjusted according to their estimated uncertainties. The variability in the output now represents the parametric uncertainty. The input-output correlations are again computed to apportion the output uncertainty into those of input parameters.

Table II DPLR input parameters to be varied for sensitivity and uncertainty analysis

Input category	Model	Parameter varied	No. of input parameters	Variability for sensitivity analysis
Dissociation reaction rates	$k=A_M T^{\eta} \exp(-D/T_a)$	A_M	40	1 order of magnitude
Exchange reaction rates	$k=A T^{\eta} \exp(-D/T_a)$	A	7	1 order of magnitude
Vibration-dissociation Coupling	$T_a = T^{\eta} T_V^{1-\eta}$	η	5	±0.15
V-T Relaxation time	Millikan and White /Camac[10]	slope	40	±10%
Binary collision integral	$\Omega^{1,1}$, $\Omega^{2,2}=A\ f(T)$	A	36	±30%
Wall Catalysis	See text	γ_{cat}, p_2	2	Entire range
			Total = 130	

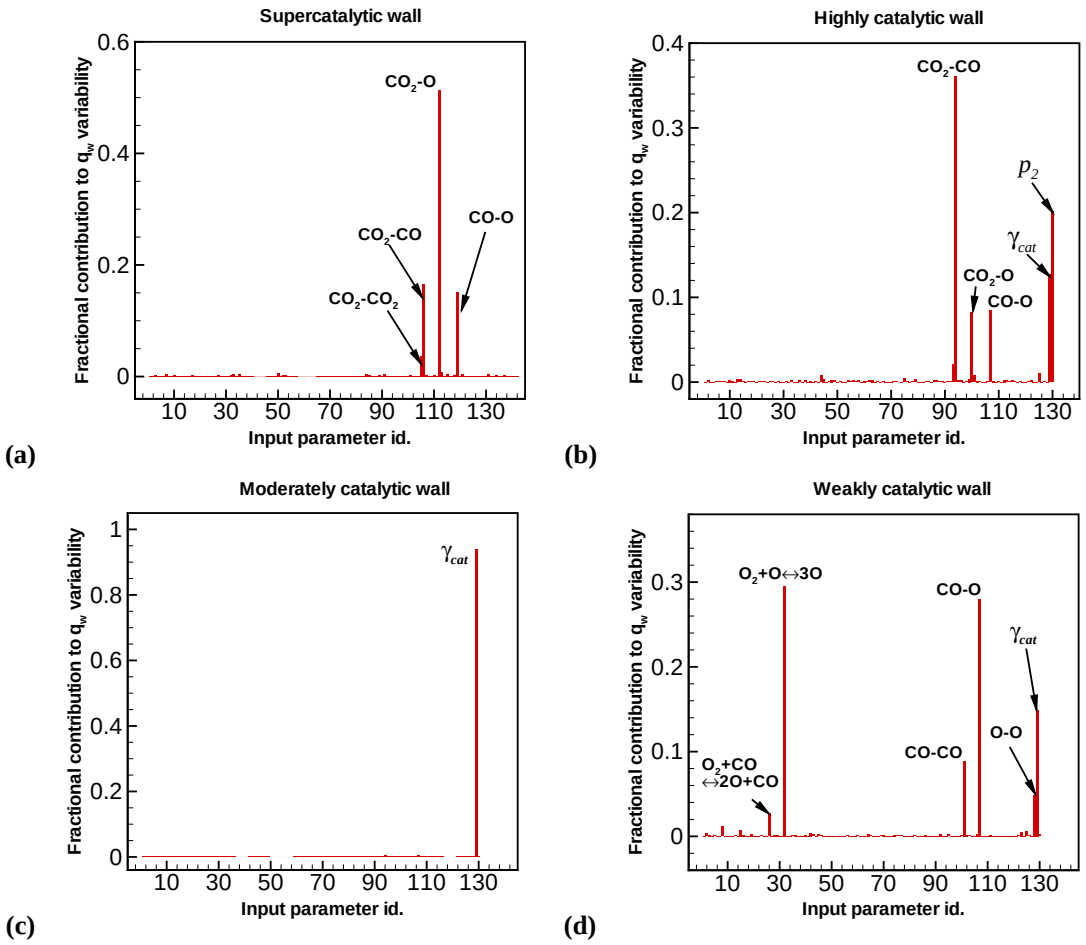

Figure 4. Fractional contributions to the heat flux variability from each input parameter. (a) Supercatalytic case, (b) highly catalytic wall, (c) moderately catalytic wall, and (d) weakly catalytic wall. The fractional contributions are determined by the square of the correlation coefficient. The binary collision integrals are labeled as species pairs.

Sensitivity Analysis

In the remainder of this paper the sensitivity and uncertainty analysis results are presented separately for each of the catalytic regimes mentioned in the prior sections. This is done since the sensitivities and the rate limiting steps at play in these regimes are significantly different. In the next few sub-sections we will present sensitivity plots in the form of bar charts with the bar heights representing the square of the correlation coefficient of each input parameter with the stagnation point heat flux q_w.

A Supercatalytic wall

Figure 4 (a) shows that in the supercatalytic case out of 130 input parameters listed in Table III, the heat flux shows sensitivity to only 4 parameters. They are all binary collision integrals as labeled in the figure. Under the assumption of a supercatalytic wall, the catalytic properties do not have any variability. The rate of CO_2 production at the wall is limited only by the diffusion transport O and CO through the boundary layer. The near wall region of the boundary layer in the steady state is however comprised mostly of CO_2 due to forced recombination. Therefore, the diffusion of O and CO in a background of CO_2 are the two major rate limiting processes, as shown by high correlation of CO_2-O and CO_2-CO collision integrals to q_w. Since the boundary layer, a small distance away from the wall, is also comprised of CO and O in addition to CO_2, the CO-O interaction also plays a role in determining the diffusion of these species toward the wall.

The heat flux also shows slight sensitivity to the CO_2-CO_2 interaction, since it controls the thermal conductivity of the near wall region. The heat flux does not show much sensitivity to the gas phase reaction rates over the range of variability considered in Table II. The reason for this insensitivity is because the freestream CO_2 is almost completely dissociated after the shock. The CO formed therein remains undissociated throughout the shock and the boundary layer. As a result not much is different, as far as the major species densities are concerned, when the gas-phase reaction rate constants are varied randomly over an order of magnitude.

B. Highly catalytic wall

In this regime we vary γ_{cat} between 10^{-1} and 10^{0} and p_2 is varied over the range of 10^{-4} to 10^{0} using a uniform distribution on a $\log_{10}$ scale. All other parameters are varied according to a Gaussian distribution. Figure 4 (b) shows the sensitivity of heat flux on various parameters in the highly catalytic regime. In this regime, both transport properties and catalytic parameters show significant correlation with the heat flux, suggesting that this regime is characterized by regions of both diffusion and surface reaction rate limiting. In a significant region of the window of variability the CO+O reaction is CO flux limited, hence the diffusion of CO in a background of CO_2 gas is one of the rate limiting steps. Other collisional interactions such as CO_2-O and CO-O are also somewhat important since in the window of variability O flux limiting also occurs as seen in Figure 3 (b). As far as the catalycity parameters are concerned, both γ_{cat} and p_2 also control the heat flux, although the effect of γ_{cat} is somewhat muted since diffusion limiting is slightly more important. However, even in a completely diffusion limited regime, the effect of p_2 is still large. This effect, as discussed earlier, is due to efficiency of utilization of all CO and O radicals in the catalytic process. If p_2 is large, most of the CO remains unused and the heat flux is low. On the other hand if p_2 is small, the heating is substantially close to maximum due to efficient utilization, although some excess O atoms are left after CO+O recombination is complete.

C. Moderately catalytic wall

As we saw earlier in Fig. 3(a), in the moderate catalytic regime, ($10^{-3}<\gamma_{cat}<10^{-1}$) the heat flux varies very strongly with the value of γ_{cat}, which is also seen in Fig. 4(c). This dependence is due to the fact that surface recombination is no longer limited by diffusion; instead the kinetic rate γ_{cat} controls the recombination. The preference parameter p_2 is less important since a full utilization of reactants CO and O does not occur due to moderate catalycity. As a result, stoichiometric requirements are not as stringent. It is also worth mentioning that since p_2 was chosen using a uniform distribution on the log scale, the low values of p_2 ($<10^{-1}$) are overemphasized. As a result the weighting on the more sensitive part of the q_w versus p_2 curve ($p_2>10^{-1}$) may be inadequate. If a uniform distribution of p_2 on a linear scale is chosen, p_2 would appear as a more sensitive quantity.

D. Weakly catalytic wall

In this regime ($\gamma_{cat} <10^{-3}$), the effect of catalycity on heating, in general, is low. The heat flux, instead, is determined primarily by direct thermal conduction from the hot gas. As a result Fig. 4 (d) shows γ_{cat} as a parameter of secondary importance. The transport properties of CO and O in a gas mixture of CO+O are important because these interactions determine the thermal conductivity of the boundary layer which is mostly comprised of CO and O (CO_2 is absent in the boundary layer due to insignificant recombination). However, the largest sensitivity of heat flux comes from the $O_2 + O \Leftrightarrow 2O + O$ gas-phase reaction. In the boundary layer this reaction proceeds in the backward (exothermic recombination) direction. The faster this reaction proceeds, more heated the boundary layer gets, which results in more thermal conduction into the wall. A slight importance of the gas phase reaction $O_2 + CO \Leftrightarrow 2O + CO$ is due to the fact that CO is also a dominant species in the boundary layer, although its rate is much smaller than that of the $O_2 + O \Leftrightarrow 2O + O$ reaction.

Input Parameter Uncertainty Estimates

A. Transport Properties

As discussed previously, the transport properties of the gas mixture, including viscosity, thermal conductivity, and binary diffusion coefficients, are computed from binary collision integral data using standard mixing rules. Collision integrals for the 36 binary interactions that occur in an 8-species CO_2-N_2

mixture were taken from the recommendations in Refs. 13 and 14. These data were collected from a variety of sources with varying accuracy. The estimated uncertainties of all 36 interactions were also reported in Refs 13 and 14; these values are employed in this work. Table III lists the uncertainties of the key binary interactions identified in the previous section.

Table III. Estimated collision integral uncertainties for key binary interactions.

Interaction	Uncertainty
CO_2–CO_2	20%
CO_2–CO	20%
CO_2–O	30%
CO–O	30%
CO–CO	20%
O–O	5%

In addition to uncertainties in the component binary interactions, additional uncertainty arises in the mixture transport properties due to non-ideal effects such as the mixture rule inaccuracies, the presence of excited state species, and nonequilibrium (non-Boltzmann) distribution of vibrational states. Therefore an additional 10% uncertainty is added to all collision integrals to account for these non-ideal effects. In this work we assume the same percentage uncertainties for both the $\Omega^{1,1}, \Omega^{2,2}$ collision integrals. This assumption is justified since the ratio of these collision integrals remains a near constant.[13,14]

B. Chemical kinetics

Out of 12 reactions considered in this mechanism, sensitivity analysis shows that only the $O_2 + M \Leftrightarrow 2O + M$ (M=O and CO) reaction shows any sensitivity in laminar convective heating as seen in Fig. 4(d). Also, this reaction occurs in the boundary layer in the reverse direction. In this work since we assume that equilibrium thermodynamic properties have no uncertainty, therefore, the uncertainty in the forward rate constant is same as that in the backward rate. The forward rate constant for this reaction was recommended by Park[22] after reinterpretation of shock tube data using a two temperature model. However, most of the experimental data points were at temperatures higher than the typical boundary layer temperature of 1500-2500 K. Although the general agreement with the experimental data is within an order of magnitude, we conservatively assign an order of magnitude uncertainty (95% confidence limit) at lower temperatures typical in the boundary layer.

Uncertainty Analysis

In this section we present the uncertainty analysis data for the 4 catalytic regimes. For each case we show a probability distribution of the stagnation point heat flux showing its uncertainty and its apportionment to the input parameter uncertainties. All input parameters that contribute less that 5% to the heat flux uncertainty are lumped into a single "other" category. Also we must emphasize that the apportionment of the heat flux uncertainty into input uncertainties assumes a near linear behavior of the model.

A Supercatalytic wall

The uncertainty due to wall catalysis is eliminated by employing a conservative supercatalytic wall assumption. Although this assumption gives the upper ceiling of the catalytic heat flux, the ceiling itself is uncertain due to uncertainties in other input parameters. Figure 5 (a) shows the probability distribution of the heat flux. The 95% confidence limits are found to be 120.6 W/cm^2 (+10.3%, -9.9%) at the stagnation point. The possibility that the supercatalytic heat flux can be larger by an additional 10.3% (of course with decreasing probability) has important design and risk mitigation consequences. Figure 5 (b) shows the apportionment of the heat flux uncertainty. As seen during the sensitivity analysis, CO_2-O collision interaction is the largest source of uncertainty to the heat flux, since this parameter controls the diffusion limited catalytic recombination rate. This is followed by other lesser important collisional interactions; CO-O and CO_2-CO. About 13% of the uncertainty is contributed by the rest of the parameters combined. This

contribution may even be less than 13% since the estimates of uncertainties of non-critical input parameters are done conservatively.

B. Highly catalytic wall

In the highly catalytic regime, the surface recombination processes approach diffusion limiting, which is apparent from a large contribution (32%) to the heating uncertainty from CO_2-CO collision integrals. However, finite rate catalycity is still a significant contributor to heat flux uncertainty. As we mentioned earlier, at high catalycity, p_2, the preference factor plays a crucial role in determining the net heat flux, and consequently appears as one of the larger contributors to the uncertainty. It is useful to emphasize that p_2 was assumed to vary over the range of $1\text{-}10^{-4}$ on a log-uniform distribution. It was also shown in Fig. 3(b) that most of the variability in p_2 caused the heat flux to remain at higher values, close to the maximum, except when p_2 is high when the heat flux rapidly drops. This causes an asymmetric probability distribution of heat flux with peak of the distribution near the higher value as seen in Figure 5 (c). The catalycity parameter γ_{cat} also contributes a 12% uncertainty because of surface process limiting at the lower end of catalycity within the confines of this regime. The 95% confidence limits for the stagnation point heat flux are 106.70 W/cm^2 (+12.0%, -17.2%).

C. Moderately catalytic wall

The uncertainty in the moderately catalytic regime ($10^{-3}<\gamma_{cat}<10^{-1}$) is dominated by the uncertainty in the value of γ_{cat} , which in this case is uniformly distributed over the entire range (in log scale). The catalytic recombination in this regime, obviously, is surface process rate limited. Also the distribution of the heat flux in Fig. 5(e) is much different from a Gaussian that is seen in other regimes. The reason for a relatively broad distribution is that the dominant input γ_{cat} is not varied according to a Gaussian distribution. Moreover, the heat flux distribution function is skewed toward the lower values. This effect occurs due to the variations caused by p_2, the preference factor. As seen in Fig 3(b), in the lower end of the moderately catalytic regime ($\gamma_{cat}\sim10^{-3}$), the effect of p_2 on heat flux is very small, which allows the heat flux values to be concentrated near the lower limit value. On the other hand a strong effect of p_2 is observed at the higher end of this regime ($\gamma_{cat}\sim10^{-1}$) due to reasons discussed earlier, which consequently causes spreading of heat flux to lower values. The 95% confidence limits for the stagnation point heat flux in this regime are 74.02 W/cm^2 (+41.0%,-33.6%), which is a wide range due to high sensitivity of heat flux to γ_{cat}. Fig 5 (f) shows, that most of the heat flux uncertainty is due to γ_{cat}.

D. Weakly catalytic wall

In the weakly catalytic regime ($\gamma_{cat}<10^{-3}$), the heat flux is dominated by conduction effects, which are controlled by the boundary layer temperature and the thermal conduction due to collisional interaction of the dominant species. Since the near wall boundary layer composition in a weakly catalytic regime is mostly CO and O, the uncertainty in CO-O collision integral appears as the largest contributor [see Fig. 5 (h)] to the heating uncertainty via thermal conductivity changes. The $O_2 + O \Leftrightarrow 2O + O$ reaction is the dominant recombination reaction in the boundary layer which results in a rise of boundary layer temperature and, consequently, a larger heat flux. The catalytic parameter γ_{cat} also contributes about 12% to the uncertainty as a sign of some catalytic heating. The overall spread of the heat flux distribution in Fig. 5 (g), however, is much smaller in this regime with the 95% confidence limits being 47.22 W/cm^2 (+11.72%, -10.59%).

Summary and Concluding Remarks

In summary, a Monte Carlo uncertainty and sensitivity analysis is performed for a moderate Mars atmospheric entry condition. As a test example, the Mars Pathfinder peak heating condition is chosen. A flux based wall catalysis model that consists of two major recombination channels, $CO+O\rightarrow CO_2$ and $O+O\rightarrow O_2$ is employed. The sensitivity and uncertainty analysis are performed for four different catalytic regimes, namely surpercatalytic, highly catalytic, moderately catalytic and weakly catalytic walls.

The sensitivity analysis found that for supercatalytic and highly catalytic regimes, the binary collision integrals are the most critical input parameters due to diffusion rate limiting. The reaction preference factor p_2 also appears as a vital input parameter at high catalycity. For moderate catalycity, a high sensitivity of

heat flux to the catalytic parameter γ_{cat} implies heterogeneous reaction rate limiting. In the weakly catalytic regime, the thermal conduction, determined by the binary collision integrals, and the O+O gas phase recombination rates appear as the most important parameters.

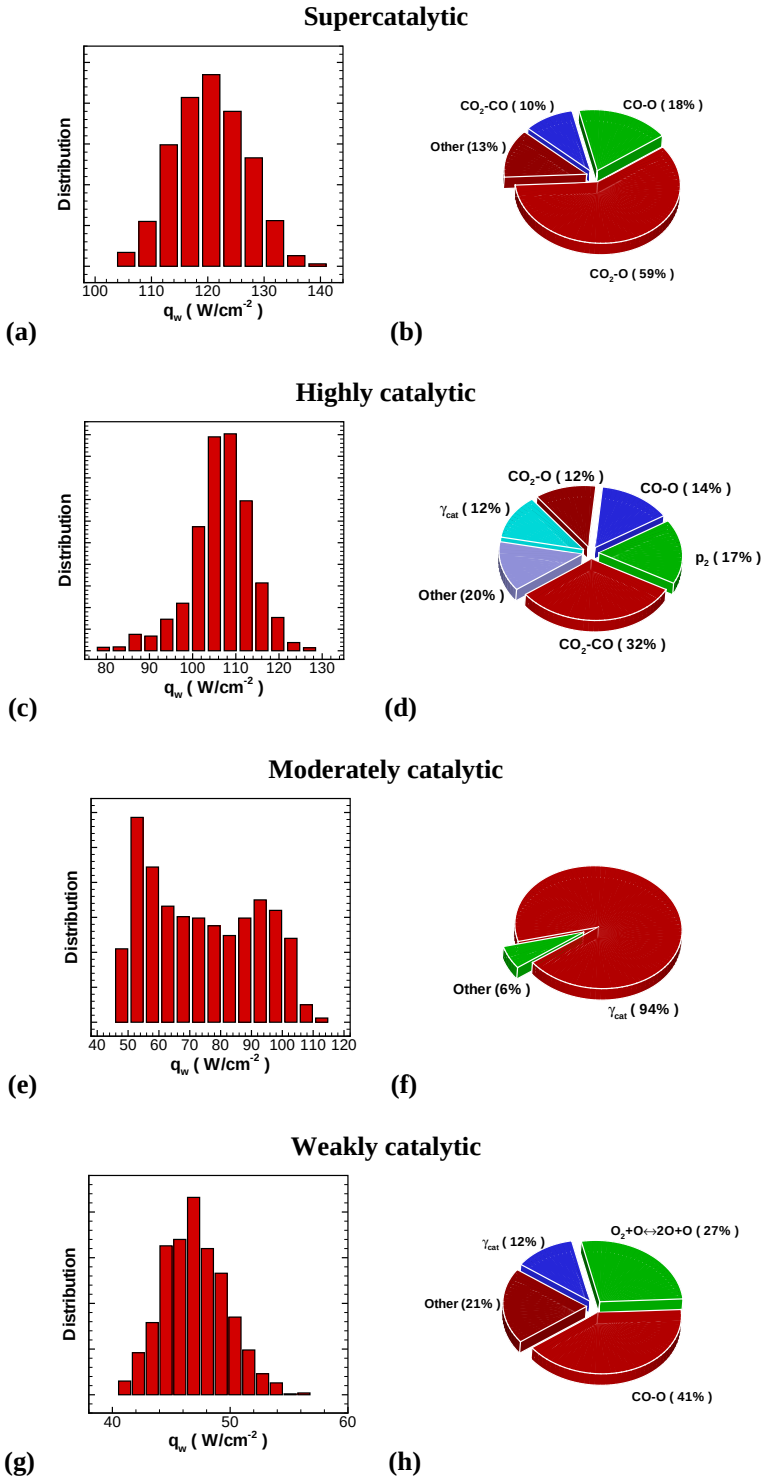

Figure 5. Stagnation point heat flux probability distributions and uncertainty contributions (a and b) supercatalytic wall, (c and d) highly catalytic wall, (e and f) moderately catalytic wall, and (g and h) weakly catalytic wall.

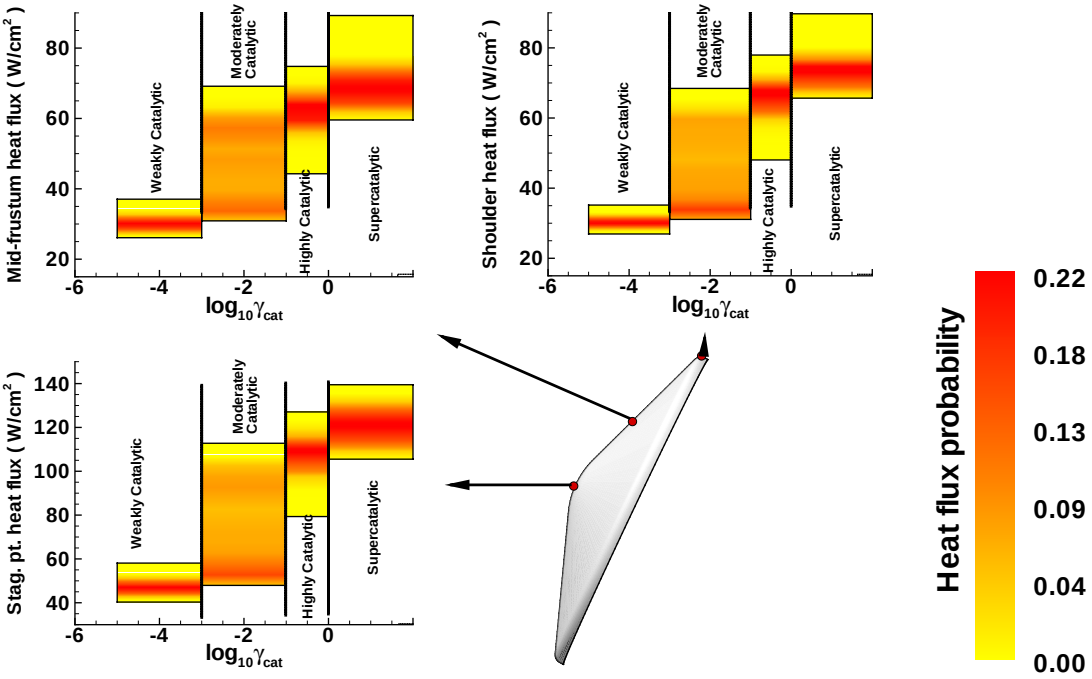

Figure 6. Stagnation point heat flux probability distribution in different catalytic regimes.

The findings of the uncertainty analysis are summed up in Fig. 6. The heat flux uncertainty is largest in the moderately catalytic condition due to a high sensitivity to γ_{cat} , which is a source of large uncertainty. In the highly catalytic regime, due to diffusion limiting, the heat flux uncertainty is reduced. Under highly catalytic and super catalytic conditions, the heat flux uncertainties are dominated by diffusion coefficient uncertainties, which, in general, contribute less to the heating uncertainty. In the highly catalytic regime, the preference parameter p_2, that controls the utilization of CO and O at the wall, is also a contributor to the uncertainty. The smallest heat flux uncertainty is found in the weakly catalytic regime (see Fig. 6), since the thermal conductivity and boundary layer temperature uncertainties are relatively lower, and the catalytic uncertainty contributes very little by definition. Figure 6 also shows heating uncertainties at mid-frustum and shoulder points in the forebody. Although the heat fluxes are lower as we move away from the stagnation point, the general uncertainty characteristics remain similar.

In conclusion, the findings of this study indicate that characterization of the catalytic properties of thermal protection material surfaces under flight conditions will result in a significantly improved heat flux prediction and consequently in a reduced heatshield margin, a lower TPS mass, or a wider choice of materials. If the surfaces are deemed highly catalytic, which is often assumed due to surface roughness, a more precise determination of the key binary collision integrals and an improved diffusion model will yield maximum improvement in the aeroheating predictions.

Acknowledgments

This work was funded by the In-Space Propulsion program under task agreement M-ISP-03-18 to NASA Ames. The work performed by Dr. Bose is supported by the prime contract NNA04BC25C to ELORET. We would also like to thank Dr. Y.K.Chen (NASA), Dr. Nagi N. Mansour (NASA), and Dr. James L. Brown (NASA) for suggesting manuscript improvements.

References

1. Johnson, L., Alexander, L., Bagett, R., Bonometti, J., Hermann, M., James, B., and Montgomery, S., "NASA's In-Space Propulsion Program: Overview and Update," AIAA Paper No. 2004-3841, July, 2004.
2. Chen, Y.-K., Henline, W. D., and Tauber, M.E., "Mars Pathfinder Trajectory-Based Heating and Ablation Calculations," *Journal of Spacecraft and Rockets*, Vol. 32, No. 2, pp. 225-230, 1995.
3. Mitcheltree, R.A., and Gnoffo, P.A., "Wake Flow about the Mars Pathfinder Entry Vehicle," *Journal of Spacecraft and Rockets*, Vol. 32, No. 5, pp. 771-776, 1995.
4. Milos, F. S., Chen, Y.-K., Congdon, W.M., and Thornton, J.M., "Mars Pathfinder Entry Temperature Data, Aerothermal Heating, and Heatshield Material Response," *Journal of Spacecraft and Rockets*, Vol. 36, No. 3, pp. 380-391, 1999.
5. Bose, D., Wright, M.J., and Gokcen, T., "Uncertainty and Sensitivity Analysis of Thermochemical Modeling for Titan Atmospheric Entry," AIAA Paper No. 2004-2455, June 2004.
6. Spencer, D., Blanchard, R., Braun, R., Kallemeyn, P., and Thurman, S., "Mars Pathfinder Entry, Descent and Landing Reconstruction," *Journal of Spacecraft and Rockets*, Vol. 36, No. 3, 1999, pp. 357-366.
7. Wright, M.J., Candler, G.V., and Bose, D., "Data-Parallel Line Relaxation Method for the Navier-Stokes Equations," *AIAA Journal*, Vol. 36, No. 9, pp 1603-1609, 1998.
8. Cheatwood, F.M. and Gnoffo, P.A., "User's Manual for the Langley Aerothermodynamic Upwind Relaxation Algorithm (LAURA)," NASA TM-4764, Apr. 1996.
9. Millikan, R. and White, D., "Systematics of Vibrational Relaxation," *Journal of Chemical Physics*, Vol. 39, No. 12, 1963, pp. 3209-3213.
10. Camac, M., "CO_2 Relaxation Processes in Shock Waves," Fundamental Phenomena in Hypersonic Flow, Edited by J.G. Hall, Cornell University Press, pp. 195-215, 1964.
11. Gurvich, L., Veyts, I., and Alcock, C., eds., Thermodynamic Properties of Individual Substances, 4th Edition, Hemisphere Publishing Corporation, New York, 1991.
12. Gupta, R., Yos, J., Thompson, R., and Lee, K., "A Review of Reaction Rates and Thermodynamic and Transport Properties for an 11-Species Air Model for Chemical and Thermal Nonequilibrium Calculations to 30000 K," NASA RP-1232, Aug. 1990.
13. Wright, M.J. and Bose, D., "Recommended Collision Integrals for Transport Property Computations II: Mars and Venus Entries," in preparation for the *AIAA Journal*.
14. Wright, M.J., Bose, D., Palmer, G.E., and Levin E., "Recommended Collision Integrals for Transport Property Computations I: Air Species," submitted to the *AIAA Journal*, Mar. 2005.
15. Ramshaw, J.D., "Self-Consistent Effective Binary Diffusion in Multicomponent Gas Mixtures," *Journal of Non-Equilibrium Thermodynamics*, Vol. 15, No. 3, 1990, pp. 295-300.
16. Park, C., Howe, J.T., Jaffe, R.L., and Candler, G.V., "Review of Chemical-Kinetic Problems of Future NASA Missions, II: Mars Entries," *Journal of Thermophysics and Heat Transfer*, Vol. 8, No. 1, pp. 9-23, 1994.
17. Wright, M.J., Olejniczak, J., Brown, J., Hornung, H., Edquist, K, "Computational Modeling of T5 Laminar and Turbulent Heating on Blunt Cones, Part 2: Mars Applications," AIAA Paper No. 2004-2455, June 2004.
18. Christmann K., Introduction to Surface Physical Chemistry, Springer-Verlag, New York, 1991.
19. Chen Y.-K., Henline, W.D., Stewart, D.A., and Candler, G.V., "Navier-Stokes Solutions with Surface Catalysis for Martian Atmospheric Entry," *Journal of Thermophysics and Heat Transfer*, Vol. 30, No. 1, pp. 32-42, 1993.
20. Sepka, S, Chen, Y.-K., Copeland, R., and Marschall, J., "Experimental Investigations of Surface Reactions in Carbon Monoxide and Oxygen Mixtures," *Journal of Thermophysics and Heat Transfer*, Vol. 14, No. 1, pp. 45-52, 2000.
21. Kolesnikov, A., Yakushin, M., Pershin, I., and Vasilevskii, S., "Heat Transfer Simulation and Surface Catalycity Prediction at the Martian Atmosphere Entry Conditions," AIAA Paper No. 99-4892.
22. Park, C., "Two-Temperature Interpretation of Dissociation Rate Data for N_2 and O_2," AIAA Paper No. 88-0458.